E6-2001-249

S. A. Karamian, J. Adam[1], D. V. Filossofov, D. Henzlova[2],
V. Henzl[2], V. G. Kalinnikov, N. A. Lebedev,
A. F. Novgorodov, C. B. Collins[3], I. I. Popescu[4], C. A. Ur[4]

ACCUMULATION OF THE ^{178m2}Hf ISOMERIC NUCLEI THROUGH SPALLATION WITH INTERMEDIATE-ENERGY PROTONS OF TANTALUM AND RHENIUM TARGETS

Submitted to «Nuclear Instruments and Methods A»

---

[1]On leave of absence: Nuclear Physics Institute, Rez, Prague, CZ-25068, Czech Republic
[2]Nuclear Physics Institute, Rez, Prague, CZ-25068, Czech Republic
[3]Center for Quantum Electronics, University of Texas at Dallas, Dallas, 75083, TX, USA
[4]National Institute of Physics and Nuclear Engineering and Induced Gamma Emission Foundation, Bucharest, 76900, Romania

1. Introduction

Experiments with high-spin, long-lived nuclear isomers, as ^{180m}Ta and ^{178m2}Hf, were recognized during the decade as an innovative test of the structure of quasiparticle nuclear states and their interaction with external radiation fields. Induced release of the energy stored in such nuclear isomers was considered as one of the most promising way for the creation of pulsed gamma-ray sources controlled by soft x-ray devices.

Triggered release of the isomer energy is very attractive for the production of powerful sources of pulsed gamma-ray radiation. For instance, 1 mg of the long-lived ^{178m2}Hf isomeric nuclei stores 1 MJ of energy in the form of the excitation energy of the isomeric state. Recent reports [1] have shown the possibility to 'stimulate' the release this energy over very short ranges of time (of the order of μsec) by exposing the material to intense low energy X-ray radiation fields. The release of this quantity of energy within let's say 1μs would produce a 1-TW flash of gamma-ray radiation in the range of 100-500 keV. The production and the practical use of such powerful sources of radiation are conditioned by the availability of the ^{178m2}Hf isomeric nuclides in large quantities.

The 31-years half-life isomeric state of the ^{178}Hf nucleus has the spin and parity 16^+ and it is located at 2.45 MeV excitation energy. This implies that ^{178m2}Hf isomeric nuclides can be produced with high yields only in nuclear reactions that proceed via intermediate states of high excitation energy and high angular momentum. The largest quantity of ^{178m2}Hf nuclei (about 10^{17}) ever produced around the world resulted from the spallation of a thick ^{nat}Ta target with 800 MeV protons, as described in Ref. [2]. The ^{nat}Ta consists practically 100% of ^{181}Ta nuclides and in the following we will simply call it Ta. The massive Ta beam dumps irradiated with the 0.4 mA proton beam at the Los Alamos meson factory, LAMPF, were chemically processed and the isolated Hf fraction contained about 100 μg of ^{178m2}Hf nuclei. The production of ^{178m2}Hf nuclei at LAMPF resulted practically as a by-product of the accelerator's operation and it was never optimized for the best purity and highest yield of this isomeric material. The LAMPF accelerator is one of the most powerful facilities in the world that can supply beam currents with intensities up to 1 mA that corresponds to a total beam power as high as 1 MW. The irradiation of thick samples with such intense beam resulted in extremely radioactive samples that needed to be cool down for a long period before they could be handled for chemical separation. An additional disadvantage of the described spallation method is the production of many Hf isotopes, stable and radioactive, with yields orders of magnitude higher than for ^{178m2}Hf. Two long-lived isotopes: ^{175}Hf ($T_{1/2}$ = 70 d) and ^{172}Hf ($T_{1/2}$ = 1.87 y) generate an intense gamma-radiation background for more than a decade. Consequently, the accumulated and chemically isolated ^{178m2}Hf could be used only after a cooling period of 20 years [1]. These contaminants can be eliminated through mass-separation techniques [3] but this process is rather difficult and results in big lose of material. For many applications, also the presence of stable ^{178}Hf material is disturbing and mass separation is not effective for removing it. The problem of separating the fraction of isomeric nuclei from the ground state nuclei of the same species is not yet solved. Some possible techniques for the specific case of ^{178}Hf were discussed in Refs. [4,5].

Samples of ^{178m2}Hf of higher purity were produced at Dubna U-200 cyclotron [6]. The reaction ^{176}Yb (^{4}He, 2n) was used with a ^{4}He-ion beam of 36 MeV energy and 100 μA intensity. Mass separation of the chemically isolated Hf fraction was also performed successfully [7] and a high-purity ^{178m2}Hf activity was isolated and used in many experiments. The isomer-to-ground state ratio was found to be about 4% that is much higher than in the case of the spallation reaction [2]. Thus, the production of ^{178m2}Hf through the (^{4}He, 2n) reaction supplies much better quality parameters than the proton-induced spallation of Ta. Unfortunately, the (^{4}He, 2n) method has 3 orders of magnitude lower absolute productivity yield compared to the spallation method due to the much lower thickness of the target layer and beam power removal problems.

The advantage of the irradiations with high-energy protons for a higher yield of ^{178m2}Hf should be generally conserved while the specific choice of the proton energy values and target geometry have to be carefully tested in order to improve the quality parameters of the produced

^{178m2}Hf activity, namely the purity and isomer-to-ground state ratio. We report in this paper the results obtained from the irradiation of Ta and ^{nat}Re targets with protons at several different energies. The measured mean cross-sections and yields of the produced radionuclides are compared in order to get the basis for the ^{178m2}Hf isomers production optimization.

Irradiations of the Ta and ^{nat}Re targets with protons were performed at the internal and external beams of the Dubna synchrocyclotron at energies of 660, 200 and 100 MeV for Ta targets and 660, 450, 300 and 150 MeV for ^{nat}Re targets. The production cross-sections for many radionuclides, including isomers, were measured by using the methods of radiochemistry and γ-ray spectroscopy. The absolute cross-section values, their variation with the number of emitted nucleons and the dependence on the proton energy were extracted and discussed from the point of view of ^{178m2}Hf isomers production. Many new and interesting conclusions concerning the reaction mechanism of the spallation with high-energy protons were drawn.

The results are compared quantitatively with the theoretical predictions of the code LAHET, which is one of the best proton-nucleus interaction codes, applied at intermediate energies. Generally, good agreement of the calculations with the measured yields was found excepting for the independent yields of nuclides near the beta-stability line. The calculations were performed separately for ^{185}Re and ^{187}Re targets (which are the two components of the ^{nat}Re with abundances of 37.4% and 62.6%, respectively) and the results were combined to get the yield values for ^{nat}Re. For Ta, the monoisotopic composition (of ^{181}Ta) was assumed.

2. Properties of nuclear reactions

When using the Ta target ^{178}Hf nuclides are populated through the ^{181}Ta(p, 2p2n) or ^{181}Ta(p, α) reactions; two protons and two neutrons are emitted from the compound system in the form of a α-particle or separately. Emission of charged particles becomes competitive with neutrons at excitation energies, E*, above 60-70 MeV. At higher excitation energies additional neutrons accompany the emission of α particles. Thus the probability for the (p, α) channel is low since for E* below ~ 70 MeV α-particle emission is suppressed by the Coulomb barrier while at higher energies appears in competition with many other (p, xn) channels. Consequently, one expects a cross-section of the (p, α) reaction to be much lower than the geometrical cross-section (≈2 barns). The yield of the ^{178m2}Hf isomeric nuclei is furthermore reduced by the isomer-to-ground state ratio.

The experimental measurement of cross-sections for reactions induced by protons in the energy range of 0.1-1.0 GeV is not yet well developed. Data are fragmentary, as reported in Ref. [8], and the known values were measured mostly in the period 1960-1970 with limited accuracy. The general behavior of the cross-sections as a function of the incident proton energy for the (p, α) reaction can be anticipated based on the results published in Ref. [9] for the ^{56}Fe(p, α) ^{53}Mn reaction. A peak cross-section of about 200 mb is reached near 60 MeV; at higher energies the cross-section decreases and a flat decrease is extended up to the GeV range. The Coulomb barrier for α-emission, in the case of Ta, is significantly higher than that for the iron target and it could result in a smoothening of the peak cross-section at low energies. This decrease of the cross-section is partially compensated by a higher total cross-section of the peripheral collisions for heavy targets (Ta) than for medium mass targets (Fe). The mechanisms of the preequilibrium emission and direct knock-out must dominate in the case of the ^{181}Ta(p, α)^{178}Hf reaction. An isomer-to-ground state ratio above 1% could be inferred based on the estimations of the angular momentum released in the reaction and taking into account the σ_m/σ_g values discussed in Ref. [6]. The present work brings more support that is experimental for the above-mentioned discussion on the isomer-to-ground state ratio.

Summarizing, cross-sections lower than 1 mb for the production of ^{178m2}Hf isomers in proton irradiation of Ta at energies in the range of (50-1000) MeV were predicted. The excitation function may have a peak placed between 60 and 110 MeV but its contribution to the integral cross-section should not be significative.

For the case of ^{nat}Re spallation with high-energy protons, nuclei with mass A = 178 are located near the maximum of the mass distribution. Even in this case the independent yield of ^{178}Hf

is orders of magnitude lower than the total yield of the A = 178 isobars because ^{178}Hf is located on the tail of the isobaric charge distribution. Unfortunately, the ^{178m2}Hf isomers result only as independent yield, directly from the reaction, while the large cumulative production of ^{178}Hf ground state is useless. Practically, the independent-to-cumulative ratio for ^{178}Hf together with the isomer-to-ground state ratio defines the obtained yield of ^{178m2}Hf. Both ratios are difficult to be predicted by calculations and our experimental results bring valuable information for the calibration of the computer code simulations.

3. Experiments

Separate irradiations of the Ta and ^{nat}Re targets with protons were performed at JINR Dubna. The proton beam was delivered by the 6 m synchrocyclotron (phasotron) of the LNP. Three Ta targets of the same thickness, 33.3 g/cm2 (about 2 cm thick), were exposed to the internal beam at different radii corresponding to incident energies of 660, 200 and 100 MeV, respectively (see Fig. 1). A fourth irradiation was performed using the extracted 660 MeV proton beam on a target consisting of a stack of two thin foils of Ta (156 mg/cm^2) and Al (30.6 mg/cm^2). This way the two foils were exposed to the same beam fluence. In the case of the ^{nat}Re irradiation, targets of 21 g/cm^2 (about 1 cm thick) thickness were exposed to the internal beam at four different incident energies, 150, 300, 450 and 660 MeV, respectively, while a stack of two foils of ^{nat}Re and Al of comparable thickness (0.56 mg/cm^2) were irradiated with the 660 MeV extracted beam. The irradiations with the extracted beam were aimed to perform the absolute calibration of the cross-section values. The cross-sections for the production of ^{7}Be and ^{22}Na through the p + Al reaction were measured with high accuracy in Ref. [10] and they were used to calibrate the cross-section of the products resulted from the irradiation of the Ta and ^{nat}Re targets.

The activity of produced Hf isomers could be determined from the thick Ta/Re targets, which were exposed to the internal beam, after chemical isolation of the Hf fraction. The activity of the samples was measured by using a coaxial HP Ge detector. The high γ-ray activity of the samples determined a high counting rate on the detector. The counting rate was optimized by varying the source-detector distance and/or inserting absorbers made of Pb, Cd and Cu such that the total dead time of the acquisition system was kept below 20% and no degradation of the good detector energy resolution (about 1.8 keV at E_γ = 1.17 MeV) was visible.

The total activity of the targets was extremely high and their chemical processing was possible only after two weeks of "cooling" the short-lived activities. The chemical separation consisted of the following operations:

1. Dissolution of the Ta/Re sample in concentrated hydrofluoric acid with addition of HNO_3;
2. Isolation of the Hf and W fractions from the bulk Ta/Re matter and from major part of other radionuclides (mostly rare-earth metals);
3. Fine rectification of the Hf fraction from the remaining Ta/Re and W substances.
4. Final purification of the Hf fraction from the Lu accumulated as a daughter of Hf radionuclides decay.
5. Isolation of the individual fractions of other elements. In the case of ^{nat}Re, they were W, Lu, and groups of heavy and light rare-earth elements.

The differential chromatography of elements in resin-filled columns and other radiochemical methods were used. Permanent monitoring of the γ-ray activity controlled the transmission of different elements through the chemical separation processes.

The ^{178}W radionuclide ($T_{1/2}$ = 21.6 d) was produced in large quantities and a fine rectification of the samples was needed to eliminate it. Its hard γ-radiation with E_γ > 1 MeV creates a high Compton background in the region of E_γ = (0.4 – 0.6) MeV, where the γ-lines of ^{178m2}Hf are placed. To measure with good accuracy the γ-rays emitted following the decay of ^{178m2}Hf one has to eliminate as much as possible the hard components from the γ-ray spectra.

A strong source of background is represented by the ^{172}Lu nuclei. They accumulate in the Hf fraction following the decay of the ^{172}Hf ($T_{1/2}$ = 1.87 y) radionuclides. The activity of the ^{172}Lu ($T_{1/2}$

= 6. 7 d) nuclides reaches the equilibrium after only few days, so that γ-ray spectra should be measured immediately after chemical separation before ^{172}Lu accumulates in the sample. This way one avoids the large background produced by the γ-ray lines emitted in the decay of ^{172}Lu and the limit of sensitivity for the estimation of ^{178m2}Hf yield is significantly improved. Finally, the statistical accuracy for the intensity of the γ-ray lines following the decay of the ^{178m2}Hf isomer was of the order of 6%.

The strongest γ-ray emitted in the decay of the ^{175}Hf nuclides has the energy E_γ = 343 keV and produces high counting rate in the Ge detector. This line was suppressed by Pb filters in front of the detector.

Since for each sample the γ-ray background was different as both intensity and composition, practically each one had its own measurement geometry and combination of absorbers. The signals from the Ge detector were sent into a high rate amplifier (ORTEC 973) and a multichannel buffer (ORTEC 921) that allowed us to increase the counting rate on the detector up to 20 kcounts/sec without a significant deterioration of the energy resolution.

The analysis of the γ-ray spectra allowed us to estimate the absolute number of radionuclides of each type by using the standard equations for radioactive decay and accumulation. The spectroscopic properties of the radionuclides were taken from the Tables of Isotopes [11,12]. The efficiency of the detector as a function of γ-ray energy was measured separately for each source-detector distance and absorber thickness by using the standard sources of ^{152}Eu, ^{154}Eu and ^{228}Th. The accuracy on the efficiency values was better than 5%. Systematical errors are due to the use of the tabulated decay properties of radionuclides. Finally, we estimated the random errors for the majority of detected radionuclides to be about 7%. This value doesn't include the error on the proton beam intensity and the calibration of the absolute yield values.

The measured number of radionuclides was transformed in production cross-section. At 660 MeV the absolute cross-section calibration was performed by using the special combined irradiation of Ta/Re and Al. For the irradiations at 100, 150, 200, 300 and 450 MeV the measured yields for the radionuclides ^{178}W, ^{185}Os and ^{183}Re, that provided intense γ-rays, could be used for absolute calibration of the cross-sections. The areas of their γ-lines were measured with high statistical accuracy in the spectra taken before chemical operations. The cross-section and the excitation function of the ^{181}Ta(p, 4n)^{178}W, ^{187}Re(p, 3n)^{185}Os and ^{187}Re(p, p4n)^{183}Re reactions were determined in Refs. [13] and [14]. The absolute calibration accuracy is estimated to be better than 15%.

4. Experimental results

The yield, Y, of a reaction product per one bombarding proton, is defined as:

$$Y = \int_{E_{min}}^{E_{max}} \sigma(E) \left(\frac{dE}{dx}\right)^{-1} dE , \qquad (1)$$

were E_{max} and E_{min} define the proton energy range in a target of known thickness, and dE/dx is the energy dependent stopping power of protons in the target material expressed in MeV/at·cm^{-2} if E is in MeV and σ in cm^2. The mean cross-section is connected with the yield through the expression:

$$\bar{\sigma} = Y \left[\int_{E_{min}}^{E_{max}} \left(\frac{dE}{dx}\right)^{-1} dE \right]^{-1} . \qquad (2)$$

Equations (1) and (2) were used for the absolute calibration of the yields and for the evaluation of $\bar{\sigma}$ in the present experiment. The resulted Y and $\bar{\sigma}$ values for Ta targets are given in Tables 1 and 2. The yield Y is given as the number of produced atoms per one bombarding proton when a 2 cm thick Ta target is irradiated. At 660 MeV bombarding energy the total range of protons in Ta is about 20 cm. The integration range for the yield estimate is determined by the 45 MeV energy loss within 2 cm of target. In the case of 200 MeV initial energy the integration range of energy is much wider, from 200 to 105 MeV. At 100 MeV, the range of protons is shorter than the thickness of the

target and only about 30% of the target's thickness is active for nuclear reactions. Thus, the energy range to be considered is defined by the individual reaction threshold and the initial energy (100 MeV). The yield and mean cross-section values, as well as the type of yield – independent or cumulative – are given in Tables 1 and 2. By independent yield we mean the number of nuclides produced directly from the reaction while the cumulative yield measures the number of nuclides resulted from the decay of the heavier unstable isobars. Some regularities can be observed from the study of the values listed in Tables 1 and 2:

1. For Hf, Lu and Tm isotopes the cumulative yields are significantly higher than the independent ones. This means that they accumulate mostly after the decay of short lived nuclides with higher Z, like W, Ta, …
2. The cumulative yields decrease at lower A values (higher number of emitted nucleons) evolving towards a rather flat behavior. Only in the case of irradiation with 100 MeV protons, the yields show a drastic decreased for $A \leq 175$.
3. The yields of Hf and Lu isomers are typically much lower than the yields of the most abundant cumulative radionuclides. This is due to the isomer-to-ground state ratio and to the low independent yield of nuclides near β-stability.
4. The yields of ^{175}Hf and ^{172}Hf are still very high at 200 MeV while at 100 MeV a decrease is noticed for ^{172}Hf.
5. Very high yield should be expected for the ground state of ^{178}Hf due to the accumulation of the ^{178}W decay products.
6. Products of two unusual reactions, namely $(p,p\pi^+)$ and (n,γ) are successfully detected. The latter one is a secondary reaction induced by the neutron flux generated in the proton interaction with the target and with the accelerator construction elements.

The data contained in Tables 1 and 2 supply a reasonable basis to discuss the productivity of the ^{181}Ta(p,α) reaction for accumulation of the ^{178m2}Hf isomeric nuclei. The fragmentary results on the ^{178m2}Hf isomer production reported in Refs. [2] and [15] were not enough for such a discussion.

In Table 3, the radionuclides detected following the irradiations at 660 MeV of Re target are listed together with their half-lives and characteristic γ-line energies. The nuclides with $T_{1/2} \leq 2$ d could not be detected due to the 3 weeks "cooling" of the targets for the reduction of the total activity. The detection limit of weak activities depends on the individual radioactive properties of a nuclide. For some cases we could measure activities corresponded to the cross-sections as low as 1 μb. The most abundant products are produced with the cross-section of the order of 100 mb. The yields and the mean cross-section values are also given in Table 3. They correspond to an average beam energy of about 645 MeV.

The data in Table 3 show that, in addition to the spallation products, many fission fragments could be also identified with moderate yields. Nuclides with masses $A < 120$ correspond to fission while those with $A > 135$ resulted from spallation processes. In the intermediate mass range $120 \leq A \leq 135$ both reaction mechanisms contribute to the yield of the same nuclide. Fission probability in the case of Re target is definitely higher than in the case of Ta.

Table 3 lists several isomers successfully detected: ^{184m}Re, ^{179m2}Hf, ^{178m2}Hf, ^{177m}Lu, ^{174m}Lu, ^{148m}Pm, ^{121m}Te, ^{110m}Ag, ^{106m}Ag and ^{91m}Nb. Their yields are typically low mostly because they are produced as independent yield directly from the reaction, while other isotopes accumulate the total yield of the isobaric chain after EC and β decays. All the abundant products result as cumulative yield.

In Table 4 the mean cross-section values measured at 450, 300 and 150 MeV are compared with the results of calculations. One can see that the fission probability decreases to lower proton energy, yet fission products can be detected even at 150 MeV. The mass range of the spallation products is shortened significantly at lower energies; for instance, at 150 MeV the nuclides lighter than ^{169}Yb were below the sensitivity limit of our detection system. Generally, the yields of the products resulting after many nucleons emission show a decreasing trend when the proton energies are lowered while the cross-section of few-nucleon emission is growing to lower energy. Such behavior is in good agreement with the theoretical predictions.

5. Model simulation of the reaction process and comparison with experimental data

Attempts to describe the cross-sections of the products from reactions with intermediate and high-energy nucleons are known in literature beginning with Ref. [16], where a first semiempirical equation was proposed and successfully applied. Later such equations were replaced by modeling of the multistep reaction process based on Monte Carlo and transport approaches (see Ref. [17]) that give a more accurate description. Many computer codes were created and a review of them can be found in Refs. [8,10] and references therein.

For the present calculations, we have chosen one the most sophisticated codes – "LAHET" [18], which appeared as a revolution of the LANL and HETC programs [19].

In the "LAHET" simulations, the reaction is described as a three-step process. The first step is represented by the intranuclear cascade (INC) when the interactions of the high-energy nucleons (or light ions) with nuclei are considered as a sequence of two body interactions between the projectile and the individual nucleons in the nucleus. The interactions of the struck nucleons with the remaining target nucleons are also treated as a sequence of two-body interactions. The projectile particle may either escape from the nucleus or it may lose its energy – through the collision with the target nucleons – and be captured in the target nuclide. Its energy is transformed in excitation energy of the residual target nucleus. The highly energetic particles promptly emitted from the nucleus during the INC stage may have enough energy to initiate further reactions with other target nuclides until their energy decrease below the cut-off energy.

The INC stage is followed by the preequilibrium emission of particles. This is an intermediate regime between the direct reaction and the statistical decay of the compound nucleus. The preequilibrium model employs an initial particle-hole configuration and excitation energy determined by the outcome of the INC cascade. At each stage of the preequilibrium model, the excited nucleus may emit neutrons, protons, deuterons, tritons, ^{3}He particles or alpha particles as the nucleon configuration evolves towards equilibrium. This process continues until the equilibrium exciton number is reached.

The evaporation model is the third step and it describes the excited residual nuclide. In this model, the deexcitation of the residual excited nuclide is described via the evaporation of nucleons and light nuclei in competition with fission.

In the present "LAHET" simulations we described the INC cascade with the ISABEL model [20], which is an extension of the VEGAS code [21]. This code accounts for nucleus-nucleus and particle-nucleus interactions as well as for interactions between particles excited above the Fermi sea.

The numerical simulations were performed for the p + ^{181}Ta and p + ^{nat}Re reactions at three values of the incident energy of 100, 200 and 660 MeV for Ta and at four values of the incident energy of 150, 300, 450 and 660 MeV for Re. In addition, at 660 MeV the yields of products were calculated separately for ^{185}Re and ^{187}Re target nuclei.

The "LAHET" code simulation was performed as described above, and for each proton energy as many as $5\text{x}10^6$ reaction events were processed. Such statistics lowers the limit of reproduced yields to about $\approx 3\cdot10^{-7}$, and defines the statistical inaccuracy of the calculated yield values in the Monte Carlo simulation. The geometry of irradiations was taken to be the same as in the experiment (see Fig. 1) and the reactions with secondary particles were taken into account. The latter process had a low probability in this geometry, especially chosen to determine physical cross-sections at well-defined energy of the bombarding protons.

The comparison of the experimental and theoretical yield values is given in the last column of Tables 1 - 4. In most of the cases, the experimental and calculated values agree within a factor 2. The agreement is worse for the case of independent or β^- cumulative yields where the discrepancy may be as high as one order of magnitude. This can be naturally explained based on the charge distribution for the spallation products. It is clear that the line of most probable charge, $Z_p(A)$, for spallation products, is located at some distance from the β-stability line, shifted towards regions of significant neutron deficiency. After series of EC decays the total yield of the isobaric nuclear chain

is converted to the longer-lived nuclide, typically placed not far from stability line. Experimentally, we measure the yields of such long-lived isotopes because we need to "cool" the target after irradiation for weeks. Thus, the cumulative yields include the most probable products of spallation, and good agreement between experiment and calculation confirms that theory reproduces well the spallation cross-sections near the maximum of charge distribution and that it describes also the mass-distribution over a wide range (from A=185 to A=140 at 660 MeV). At lower proton energies, the total mass range for the spallation products is shortened but the mass distribution is still well reproduced.

The nuclides near the β-stability line, identified experimentally, can be produced only as independent or β^- cumulative yield. For them the agreement between theory and experiment is worse. Nevertheless, one has to be aware that these nuclides are placed on the tail of the charge distribution of their isobars, far from the most probable charge $Z_p(A)$, and they correspond to low yields, sometimes at the limit of the accuracy of our measuring technique.

Unfortunately, all the isomers of interest, like ^{178m2}Hf, ^{179m2}Hf and ^{177m}Lu, correspond to nuclides near the β-stability line and their independent yields could not be predicted well by theory. Furthermore, the present version of the model simulation does not include the calculation of the isomer (m) to ground state (g) ratio; only the total yield (g + m) of the nuclides can be estimated with limited accuracy. Our new experimental data on the isomer production through spallation reactions are a unique source of data useful for clarifying the problem. From the results listed in Tables 1-4, one can estimate experimentally some isomer to ground state ratios. For isomers that have lower spins (6ħ): ^{184m}Re, ^{174m}Lu and ^{148m}Pm, values of $\sigma_m/\sigma_g \approx 1.0$ are typical. For higher spin isomers as ^{179m2}Hf (25/2ħ), ^{178m2}Hf (16ħ) and ^{177m}Lu (23/2ħ), the ratio is lower being of the order of 0.01 - 0.1. Such estimations are not very accurate because they make use of the calculated total yield of the nuclides. In addition, we have to consider the uncertainties on the measured yields of the isomeric states that are of the order of 20-30%.

The calculated yields and cross-sections for fission fragments are also compared with experimental results in Tables 1-4. The agreement is in general worse than for the spallation products. At 660 MeV the simulation is adequate, at least schematically, but at lower proton energies the discrepancy reaches one order of magnitude. It means that the simulation code systematically underestimates the probability of fission at E_p<400 MeV for Ta and Re targets. At 660 MeV, the yields of ^{106m}Ag and ^{110m}Ag isomers can be compared with the calculated ones for these nuclides resulted as fission products. High values of the isomer-to-ground state ratio are obtained for them as expected from the relations between the isomer spin and mean angular momentum of fission fragments.

Some regular trends could be deduced from the analysis of the experimental and calculated yield values. The mass-distribution plot of the reaction products can reveal some of them. The cumulative yields of long-lived isobars are well defined both in experiment and in theory. Their yields are plotted in Fig. 2 as a function of the missing mass number $(-\Delta A) = A_t + 1 - A_p$, where A_t and A_p are the mass numbers of the target and product nuclides, respectively. Practically, $(-\Delta A)$ corresponds to the number of nucleons emitted in the reaction and it shows how far the product nucleus is shifted from the compound nucleus on the A axis. Likewise, one can use $(-\Delta Z) = Z_t + 1 - Z_p$ instead of $(-\Delta A)$ to show how many units of nuclear charge were released in the reaction. The parametrization in $(-\Delta Z)$ is useful only when the independent yields of radionuclides are discussed, because after β^+ and EC decays, the Z number of the products changes and their yields are integrated in the cumulative yield of the longest-lived nuclide within the isobaric chain of a given A value. Unfortunately, it is difficult to detect many isobars and consequently the analysis of the charge-distribution of isobars is based only on the theoretical values. At the same time, the mass-distribution is not distorted by the decay of the radionuclides and the cumulative yields are plot both for experimental and theoretical values.

In Fig. 2a the mass-distribution for the p + ^{181}Ta reaction at 660 MeV is shown. Both the experimental and the theoretical values show a similar behavior. The systematic deviation, of a factor about 1.3, is observed near the maximum of the distributions. In Fig. 2b we plotted the mass-

distribution for the case of ^{nat}Re target at 660 MeV. The distributions look very similar in Figs.2a and 2b.

To estimate the yield of ^{178m2}Hf isomer theoretically, one needs to know the independent yield of this product. In Fig. 3, the calculated isobaric charge-distributions for ^{181}Ta and ^{187}Re targets are shown. The ^{178}Hf nuclide, being produced in the p + ^{187}Re irradiation, is located on the tail of the charge-distribution because the maximum of the distribution is shifted towards neutron deficient isotopes (as ^{178}W in this case). The ^{178}W nuclide, after EC decay with a half-life of $T_{1/2}$ = 21.6 d, populates ^{178}Ta and then ^{178}Hf but only in the ground state. It results that one needs to separate the Hf fraction from the samples before the decay of ^{178}W contributes to the degradation of the isomer-to-ground state ratio. This conclusion is valid both for the Ta and the Re targets.

Satisfactory agreement between theory and experiment was found for cumulative yields but this does not ensure the description of the individual independent yields of nuclides with the same success, especially, when they are far from the maximum of the charge-distribution. From Table 1 one can see that the yield of neutron-rich isotopes (e.g. ^{166}Dy, ^{160}Tb, ^{148}Pm, and ^{140}Ba) is significantly underestimated by calculations. The irradiation of ^{181}Ta at 660 MeV produced many Eu isotopes and their detection may bring additional information on the independent yields. In Fig. 4 the cumulative and independent yields of Eu isotopes are shown. Again, it can be noticed that the yield of the neutron-rich ^{156}Eu is not reproduced by the calculation, the discrepancy being as high as one order of magnitude. In the case of the independent yields of lighter isotopes, the agreement is good for A=148 and 149, but not for A=146. Cumulative yields are better reproduced.

Finally, one concludes that the independent yields of radionuclides are not well described by the calculations and for nuclides with Z/A ratio that deviates from the line of most probable Z/A the predictions are unreliable. The same is true also for fission fragments, especially, at proton energies <400 MeV.

6. Angular momentum distribution and isomer-to-ground state ratios

Isomer-to-ground state ratios in reactions at intermediate energies were measured and discussed in Refs. [8,10,22-24] and references therein. Qualitatively, it was concluded that high spins could be populated not only in reactions with protons but also by π-meson capture.

As discussed in the previous section, the independent and cumulative yields of radionuclides could be simulated with reasonable accuracy using theoretical models and the corresponding numerical codes. One of them ("LAHET") was applied for the present calculations. Nevertheless, such codes do not reproduce the isomer-to-ground state ratios (σ_m/σ_g) because of the following reasons: 1) difficulties in calculating the angular momentum (l) distribution for the reaction residues, and 2) uncertainties in the prediction of the σ_m/σ_g values even for known l distribution. Some models, aimed to solve the problem "2", were discussed in literature [25] but the results of such theoretical calculations are sensitive to the choice of numerical parameters. Problem "1" is even less investigated, especially, in the case of reactions induced by nucleons in the range of intermediate energies (100-1000 MeV). Thus, for the moment, the prediction of the σ_m/σ_g ratio should be based mostly on experimental results and semiempirical arguments. Ref. [26] proposed such a systematics in the range of low energies and it was shown that the isomer-to-ground state ratio is determined mostly by the angular momentum of the reaction product.

The results obtained from the p + Ta reaction at proton energies of 100, 200 and 660 MeV allowed us to determine experimentally the isomer-to-ground state ratios for the ^{174}Lu and ^{148}Pm nuclides. Only for these two nuclides the "m" and "g" states were independently populated. For both nuclides the ground state has spin and parity 1^- while the isomeric state has 6^-. The σ_m/σ_g values measured at 660 MeV are given in Table 5. It can be seen that they exceed unity meaning that the isomeric 6^- state is populated with higher yield than the 1^- ground state. A similar situation is observed also at 200 and 100 MeV irradiation energies (see Table 2) but with a decreasing trend of the σ_m/σ_g values to lower bombarding energy. For the other isomers listed in Table 5 only the independent yield of the isomeric state could be measured experimentally and for the ground states

we used the values estimated with "LAHET". The ground state independent yields for these nuclides could not be measured due to the large cumulative component. Our experimental set-up was based on γ-ray spectroscopy methods that cannot be used for measuring the yields of stable isotopes that do not decay γ.

To understand the results given in Table 5, one has to analyze the properties of the angular momentum distribution for the reaction products. Then, based on empirical systematics one can evaluate the corresponding σ_m/σ_g values. Of course, such an estimate is not very accurate and it allows only for a qualitative discussion. For the purpose of such a discussion, let us consider the spallation reaction as a two steps process: 1) the primary momentum transfer at the collision and 2) emission of particles. During the first step, the colliding proton transfers linear and angular momentum to the target nucleus. In the second step, the excited nucleus emits many nucleons corresponding to the INC cascade, the preequilibrium and the evaporation stages (see Section 5 for details). After nucleons are emitted, the angular momentum vector l_f is defined by the initially transferred angular momentum l_i and by the angular momentum accumulated due to the nucleon emission. Finally, the cascade of γ-quanta and conversion electrons removes the residual angular momentum and excitation energy populating the ground and isomeric states.

At the impact of 660 MeV protons with a Ta/Re target nucleus a maximum angular momentum of about 40 $\hbar$ can be released. This value corresponds to the transfer of a total linear momentum at the maximum impact parameter defined by the radius of nucleus: $b_{max} = r_0 A^{1/3}$. The probability of such transfer is low because the momentum Δp transferred in peripheral collisions is typically much lower than the total momentum of the projectile. The linear momentum of the projectile can be absorbed completely in head-on collisions but this does not produce large angular momentum since $l_i = \Delta p \cdot b$, and $b \approx 0$ at the head-on impact. Thus, one has to assume low angular momentum transfer both at the tangential and at the head-on collisions, while at values of the impact parameter $b \approx b_{max}/2$ angular momenta $l_i \approx$ (10-20) $\hbar$ can be reached with high probability.

The transferred linear momentum Δp should be a decreasing function of the impact parameter. Since the number of emitted nucleons (-ΔA) is proportional to the excitation energy $E^* \sim (\Delta p)^2$, one deduces that low (-ΔA) values correspond to the peripheral collisions and the highest (-ΔA) to the head-on collisions. Summarizing, the average angular momentum $\langle l_i \rangle$ transferred on the first step of the reaction depends on the (-ΔA) parameter like schematically shown in Fig. 5a.

Let consider now the second step of the process. What happens with the angular momentum distribution on the stage of the nucleon emission? At the nuclear temperature of about 3 MeV each nucleon carries away an average angular momentum $|\Delta l| \approx 3\ \hbar$, when emitted. The random orientation of the Δl vectors of many nucleons leads to a wide angular momentum distribution after their summation. The width of the distribution is proportional to $\sqrt{(-\Delta A)}$. When the initial l_i is nearly zero, after the cascade emission stage, the average l_f value grows significantly and arrives to be of the same order of magnitude as the width of the distribution, i.e. of about ~ 10 $\hbar$ after emission of (10-15) nucleons. However, when l_i is as high as (10-20) $\hbar$, the center of gravity of the distribution remains almost stable and only its width increases significantly. If $l_i >$ (25-30) $\hbar$, the nucleon emission removes angular momentum from the system and $\langle l_f \rangle$ decreases.

This behavior is the result of two different characteristics of the de-excitation process. The random combination of many individual vectors leads to an increase of the module of the sum vector because the phase volume in the spin space is proportional to the $(2l + 1)$ factor. At the same time, the level density factor has the opposite influence on the resulting spin after summation. These two effects compensate each other when the initial spin of the heavy nucleus is within the range of (10-20) $\hbar$. At low l_i values, the phase volume factor is dominant and $\langle l \rangle$ is growing up due to the combination of many individual vectors of emitted nucleons. On the contrary, at $l_i >$ (25-30) $\hbar$ the level density factor leads to a decrease of the initial spin.

In the case of 660 MeV protons colliding with the Ta nucleus, the initial angular momentum is typically in the range of $l_i \approx$ (5-20) $\hbar$, depending on the impact parameter or (-ΔA) value. Thus, the cascade nucleon emission influences mostly the width of the distribution. Since the number of

emitted nucleons is about (-ΔA) = 10, the initially transferred angular momentum should be of about (10-15) $\hbar$, and then the 10 emitted nucleons produce a broadening of the spin distribution, as it is shown in Figs. 5b and 5c. Finally, the spin distribution covers a range of angular momenta from 0 to 25 $\hbar$.

The final angular momentum distribution shown in Fig. 5c should give a realistic estimation of the σ_m/σ_g value in the case of ^{178m2}Hf production when irradiating ^{187}Re with 660 MeV protons (when (-ΔA) = 10). In the case of p + Ta irradiations the mean ℓ value is much lower for the A = 178 products.

When the number of emitted nucleons is small (-ΔA = 3-5), as in the reactions with Ta, for isomers as ^{179m2}Hf, ^{178m2}Hf and ^{177m}Lu, the isomeric-to-ground state ratio is expected to be much lower than unity, because of the small transferred angular momentum and the high spin of the isomers, 25/2, 16 and 23/2 $\hbar$, respectively. The σ_m/σ_g values given in Table 5 are in good agreement with this prediction. It can be concluded that the estimates of the isomer-to-ground state ratios using the calculated independent yields look reasonable. We have also to mention that until now the isomer-to-ground state ratios for these high-spin isomers populated in reactions with 660 MeV protons were unknown. The present work put some light on this important subject. In practice, for most of the cases the yield of the ground state is much higher (due to the cumulative process) than the one of the isomeric states resulting in low σ_m/σ_g values. As discussed above, the separation of ^{178}Hf from ^{178}W is necessary in order to improve the final σ_m/σ_g ratio.

The expectation in the case of Re targets was that higher angular momenta are produced for the A = 178 isobars compared with the case of Ta targets. This would have resulted in an increase of the isomer-to-ground state ratio for nuclides with high-spin isomers. However, the calculations reported in Tables 3 and 4 show that the total independent yield (m + g) for these nuclides is low. Finally, measured production of ^{178m2}Hf through the p + Re reaction is lower than what we obtained from the p + Ta reaction at similar proton energies.

7. Choice of the optimum variant for the ^{178m2}Hf production

Table 6 compares the results for ^{178m2}Hf production through the spallation of Ta and Re targets with high-energy protons. It can be noticed that Re targets does not provide any advantage compared to the use of Ta target, neither in productivity, nor in the reduction of the ^{172}Hf impurity. This impurity is the most disturbing one due to its long half-life ($T_{1/2}$=1.87 y) and very reach γ-ray spectra of the daughter nuclide ^{172}Lu (6.7 d). At the lowest energy, 150 MeV, the yield of ^{172}Hf in the p + Re reaction is significantly reduced but the ^{178m2}Hf isomer cross-section decreases too. This comparison shows that the use of Ta targets is more advantageous than the Re targets.

The mean cross-sections measured in the present work are not in complete agreement with the fragmentary data reported in Refs. [2,8,15]. Some discrepancies can be explained by different geometry of irradiations. In Ref. [2], the experiment is described schematically, and that does not allow an accurate comparison. The contribution from the reactions induced by secondary neutrons and charged particles can be significant, especially in the geometry of thick massive beam dump. It is reasonable to assume that the total reaction cross-section is of the order of the geometrical cross-section of the Ta nucleus (≈2 barn). Then, the nuclear interaction range should be of about 10 cm in Ta that is shorter than the total range of 800 MeV protons (25 cm) due to the electronic stopping power. If we further assume that the average neutron multiplicity per nuclear interaction is $\nu \geq 2$, one can conclude immediately that the number of neutrons in the target is much larger than the number of bombarding protons. Consequently, the neutron-induced reactions were very important in the geometry of the beam dump at LAMPF.

The mean cross-section for the production of ^{178m2}Hf isomers has an almost flat dependence on the proton energy so that the main problem concerning the production is the contaminants production. At the lowest irradiation energy, 100 MeV in the case of the p + Ta reaction, the production cross-sections of ^{175}Hf and ^{172}Hf decrease but they are still order of magnitude higher

than ^{178m2}Hf. Production of Hf isomers with protons of low energy has many advantages: easier operation of the accelerator, less isotopes produced in the target and consequently lower radioactivity level. At the same time, we have to notice that at the higher irradiation energy the yields of the main contaminants decrease again while the one for the Hf isomer has a slight increase.

Let us consider the case of the proton irradiation of a Ta target with 100 MeV protons at a beam current of 150 μA. The target thickness should be taken of about 0.7 cm in order to cover the active energy range. Assuming the beam diameter of about 2 cm, one can find that the beam releases about 8 kW thermal power in the Ta targets of 35 g weight. Such thermal power density can be removed without problems. Based on the results given in Table 2, one deduces a productivity on the level of 10^{10} atoms of ^{178m2}Hf per second, or 2 μg per week of irradiation. The yield of ^{172}Hf is 100 times larger and that of ^{175}Hf is 1400 times larger. The latter isotope completely decays out after 2 years of cooling. In order to improve the isomer-to-ground state ratio it is recommended to perform the irradiation for one week only and afterwards to perform the chemical isolation of Hf. This way one avoids the accumulation of ground state ^{178}Hf due to the ^{178}W EC decay. Also, the accumulation of ^{179}Hf stable isotope is reduced by the removal of its precursor, ^{179}Ta.

At 100 MeV the absolute productivity of ^{178m2}Hf isomer is 10 times lower than at 660 MeV but it is by a factor 50 higher then it was possible to reach using the ^{176}Yb(^{4}He,2n) reaction [6]. The quality parameters appear as follows: the presence of ^{172}Hf is lower at 100 MeV than at 660 MeV and the isomer-to-ground state ratios are comparable at both energies. Based on the results obtained from our measurements at 100 MeV and the previous ones from the LAMPF facility [2], we can conclude the following:

1. The use of thin targets results in lower total activity and less variety of produced radioisotopes. This moderates the safety problems for the processing of the irradiated targets. The cooling time needed for the ^{172}Hf activity to reduce at the level of the ^{178m2}Hf activity was changed from 20 yrs. in the case of the samples irradiated at LAMPF at about 6 yrs. for the samples irradiated by us.
2. The use of samples (30-50) times lighter than in the case of LAMPF also offers more convenience for the chemical separation of the various isotopes.
3. We can divide the contaminants in two main categories: a) isotopes, as ^{172}Hf and ^{175}Hf, that cannot be chemically separated from ^{178}Hf and produce high radioactivity of the samples, and b) isotopes, as ^{178}W, that degrade the isomer-to-ground state ratio due to their decay to the ground state of ^{178}Hf. One has to optimize the production process to minimize the presence of the first category of contaminants. As shown at the first point this goal was achieved. To eliminate the second category of contaminants one has to periodically change the targets and to separate the Hf fraction.
4. The operation costs for small accelerator that can supply protons of 100 MeV are significantly lower that the ones for high-energy accelerators. Moreover, small sized accelerators are available in many laboratories around the world.

Our study shows that the production of grams or even milligrams of the ^{178m2}Hf isomer is still open to discussion. What we have clearly showed is that the p + Ta reaction is more prolific than the p + Re one. The relatively low cross-section for ^{178}Hf production at 660 MeV both for Re and Ta targets is mostly due to the position of this nuclide far from the line of most probable spallation products, $Z_p(A)$. The only way to overcome this difficulty is to use a target nucleus as rich as possible in neutrons. A survey of the neighboring isotopes available in nature has revealed as a good candidate the ^{186}W nuclide.

8. Summary

The yields of radionuclides produced through proton irradiations of Ta/Re targets were measured by using the γ-ray spectroscopy methods to identify the γ-rays emitted from the chemically isolated fractions. About 65 nuclides were identified from the samples irradiated at 660

MeV and the mass-distribution of the spallation and fission products was successfully evaluated. Similar results were obtained at the other proton energies: 450, 300, 200, 150 and 100 MeV, respectively. Several isomers were populated during the irradiations and allowed us to estimate isomer-to-ground state ratios that we compared with a semiempirical ansatz. Based on our experimental results and on previous data, as well, we addressed the problem of optimization of ^{178m2}Hf production and accumulation.

Acknowledgements

The authors express their gratitude to the LNP synchrocyclotron staff for the irradiation of targets, and to P.Chaloun for the assistance in measurements. This work was supported by the U.S. Air Force European Office of Aerospace Research and Development under contracts No. F61775-99-WE030 and No. F61775-00-WE056 with the IGE Foundation.

Table 1. Yields of radionuclides and mean cross-sections measured after activation of a Ta target of 33.3 g/cm^2 thickness by 660 MeV protons. The comparison with theory prediction is given at the last column. The energy range is from 660 to 615 MeV for all reactions.

Nuclide	$T_{1/2}$	E_γ, keV	Type of yield	Mean σ, mbarn	Yield value *), atoms/proton	Y_{theor}
**) ^{182}Ta	115 d	1231.0	Indep.	-	$0.85\cdot10^{-3}$	-
**) ^{181}Hf	42.4 d	482.0	Indep.	0.14	$1.7\cdot10^{-5}$	$2.8\cdot10^{-5}$
^{179m2}Hf	25.1 d	453.7	Indep.	0.52	$5.8\cdot10^{-5}$	$1.5\cdot10^{-3}$ ***)
^{178}W	21.6 d	1340.9	Indep.	5.9	$6.6\cdot10^{-4}$	$9.3\cdot10^{-4}$
^{178m2}Hf	31 y	574.2	Indep.	0.31	$3.5\cdot10^{-5}$	$1.7\cdot10^{-3}$ ***)
^{177m}Lu	161 d	418.5	Indep.	0.25	$2.8\cdot10^{-5}$	$3.0\cdot10^{-4}$ ***)
^{175}Hf	70 d	343.4	EC cum.	56	$6.2\cdot10^{-3}$	$4.9\cdot10^{-3}$
^{174g}Lu	3.31 y	1241.8	Indep.	2.5	$2.8\cdot10^{-4}$	} $4.8\cdot10^{-4}$
^{174m}Lu	142 d	992.0	Indep.	3.0	$3.3\cdot10^{-4}$	
^{173}Lu	1.37 y	272.2	EC cum.	61	$6.7\cdot10^{-3}$	$5.5\cdot10^{-3}$
^{172}Hf	1.87 y	1093.6	EC cum.	47	$5.2\cdot10^{-3}$	$4.6\cdot10^{-3}$
^{172}Lu	6.7 d	1093.6	Indep.	8.1	$0.9\cdot10^{-3}$	$0.83\cdot10^{-3}$
^{171}Lu	8.22 d	739.8	EC cum.	65	$7.2\cdot10^{-3}$	$5.4\cdot10^{-3}$
^{170}Lu	2.0 d	985.1	EC cum.	64	$7.1\cdot10^{-3}$	$5.3\cdot10^{-3}$
^{169}Yb	32.0 d	307.7	EC cum.	69	$7.6\cdot10^{-3}$	$5.5\cdot10^{-3}$
^{168}Tm	93.1 d	720.3	Indep.	1.3	$1.5\cdot10^{-4}$	$7.0\cdot10^{-5}$
^{167}Tm	9.24 d	531.5	EC cum.	66	$7.3\cdot10^{-3}$	$4.9\cdot10^{-3}$
^{166}Yb	2.36 d	1374.1	EC cum.	42	$4.6\cdot10^{-3}$	$5.4\cdot10^{-3}$
^{166}Dy	3.4 d	1379.6	β^- cum.	1.8	$2.0\cdot10^{-4}$	-
^{160}Tb	72.3 d	1271.9	Indep.	0.10	$1.2\cdot10^{-5}$	-
^{156}Tb	5.35 d	534.3	Indep.	0.48	$5.3\cdot10^{-5}$	$4.6\cdot10^{-5}$
^{155}Tb	5.32 d	367.4	EC cum.	32	$3.5\cdot10^{-3}$	$3.1\cdot10^{-3}$
^{156}Eu	15.2 d	2097.7	β^- cum.	0.12	$1.3\cdot10^{-5}$	-
^{153}Gd	242 d	103.2	EC cum.	22	$2.4\cdot10^{-3}$	$2.5\cdot10^{-3}$
^{151}Gd	120 d	243.2	EC cum.	19	$2.1\cdot10^{-3}$	$2.2\cdot10^{-3}$
^{149}Gd	9.4 d	298.5	EC cum.	27	$3.0\cdot10^{-3}$	$2.0\cdot10^{-3}$
^{149}Eu	93.1 d	277.0	EC cum.	28	$3.1\cdot10^{-3}$	$2.1\cdot10^{-3}$
^{148}Eu	54.3 d	550.3	Indep.	0.73	$0.8\cdot10^{-4}$	$1.6\cdot10^{-4}$
^{148g}Pm	5.37 d	914.9	Indep.	0.045	$5\cdot10^{-6}$	} $1.0\cdot10^{-6}$
^{148m}Pm	41.3 d	286.6	Indep.	0.067	$7.5\cdot10^{-6}$	
^{147}Eu	24.6 d	601.4	EC cum.	15	$1.68\cdot10^{-3}$	$1.5\cdot10^{-3}$
^{146}Gd	48.3 d	633.7	EC cum.	14	$1.54\cdot10^{-3}$	$1.2\cdot10^{-3}$
^{146}Eu	4.6 d	633.7	Indep.	0.5	$5.4\cdot10^{-5}$	$3.8\cdot10^{-4}$
^{145}Eu	5.94 d	893.7	EC cum.	8.5	$0.94\cdot10^{-3}$	$1.2\cdot10^{-3}$
^{144}Pm	363 d	476.8	Indep.	≤1.7	$\leq2\cdot10^{-4}$	$6.9\cdot10^{-5}$
^{143}Pm	265 d	742.0	EC cum.	5.8	$6.5\cdot10^{-4}$	$8.8\cdot10^{-4}$
^{140}Ba	12.75 d	1596.5	β^- cum.	0.010	$1.2\cdot10^{-6}$	-
^{139}Ce	137.7 d	165.8	EC cum.	2.4	$2.6\cdot10^{-4}$	
^{136}Cs	13.16 d	1048.1	Indep.	≤0.011	$\leq1.3\cdot10^{-6}$	-
^{133}Ba	10.5 y	356.0	EC cum.	0.7	$8\cdot10^{-5}$	$9.6\cdot10^{-5}$
^{131}Ba	11.8 d	496.3	EC cum.	0.94	$1.0\cdot10^{-4}$	$7.5\cdot10^{-5}$

Nuclide	$T_{1/2}$	E_γ, keV	Type of yield	Mean σ, mbarn	Yield value *), atoms/proton	Y_{theor}
^{113}Sn	115 d	391.7	EC cum.	0.11	$1.2 \cdot 10^{-5}$	$6 \cdot 10^{-6}$
^{110m}Ag	250 d	884.7	Indep.	0.04	$4.3 \cdot 10^{-6}$	$1.5 \cdot 10^{-6}$ ***)
^{106m}Ag	8.46 d	1045.8	Indep.	0.07	$0.8 \cdot 10^{-5}$	$4 \cdot 10^{-6}$ ***)
^{105}Ag	41.3 d	443.4	EC cum.	0.27	$2.5 \cdot 10^{-5}$	$1 \cdot 10^{-5}$
^{102}Rh	207 d	475.1	Indep.	0.08	$7.2 \cdot 10^{-6}$	$7 \cdot 10^{-6}$
^{101}Rh	3.3 y	198.0	β^+ cum.	0.31	$2.9 \cdot 10^{-5}$	-
^{100}Pd	3.6 d	2376.1	β^+ cum.	0.028	$2.7 \cdot 10^{-6}$	$6 \cdot 10^{-6}$
^{95}Zr	64 d	756.7	β^- cum.	0.12	$1.3 \cdot 10^{-5}$	$2.5 \cdot 10^{-6}$
^{95}Nb	35 d	765.8	Indep.	0.22	$2.1 \cdot 10^{-5}$	$6 \cdot 10^{-6}$
^{91m}Nb	62 d	1204.8	Part. cum.	0.13	$1.5 \cdot 10^{-5}$	$2 \cdot 10^{-5}$ ***)
^{88}Zr	83.4 d	392.9	EC cum.	0.14	$1.6 \cdot 10^{-5}$	$2.2 \cdot 10^{-5}$
^{88}Y	106.6 d	1836.0	Indep.	0.33	$3.7 \cdot 10^{-5}$	$1 \cdot 10^{-5}$
^{87}Y	3.35 d	388.4	β^+ cum.	0.35	$3.9 \cdot 10^{-5}$	-
^{85}Sr	64.8 d	514.0	β^+ cum.	0.45	$5.0 \cdot 10^{-5}$	$2.4 \cdot 10^{-5}$
^{84}Rb	32.9 d	881.6	Indep.	0.34	$3.7 \cdot 10^{-5}$	$1.2 \cdot 10^{-5}$
^{83}Rb	86.2 d	520.4	β^+ cum.	0.47	$5.2 \cdot 10^{-5}$	$3.6 \cdot 10^{-5}$
^{75}Se	120 d	264.6	β^+ cum.	0.42	$4.6 \cdot 10^{-5}$	$2 \cdot 10^{-5}$
^{74}As	17.8 d	595.8	Indep.	0.32	$3.5 \cdot 10^{-5}$	$1.9 \cdot 10^{-5}$
^{72}Se	8.4 d	834.0	β^+ cum.	0.09	$1.0 \cdot 10^{-5}$	$2.5 \cdot 10^{-6}$
^{65}Zn	244 d	1115.8	β^+ cum.	0.3	$3.3 \cdot 10^{-5}$	$1.7 \cdot 10^{-5}$
^{60}Co	5.27 y	1332.5	Indep.	0.014	$1.6 \cdot 10^{-6}$	-
^{59}Fe	44.5 d	1099.5	β^- cum.	0.18	$2.0 \cdot 10^{-5}$	$1 \cdot 10^{-5}$
^{56}Co	78.8 d	2598.6	EC cum.	0.027	$3.0 \cdot 10^{-6}$	$2 \cdot 10^{-6}$
^{52}Mn	5.6 d	1434.1	β^+ cum.	0.018	$1.9 \cdot 10^{-6}$	$1 \cdot 10^{-6}$
^{48}V	16 d	1312.1	EC cum.	0.023	$2.5 \cdot 10^{-6}$	$4 \cdot 10^{-6}$

*) Random errors are within ±7%, and the standard error of the absolute calibration is of about ±15%;

**) ^{182}Ta and ^{181}Hf are produced in the reactions (n,γ) and (p,pπ$^+$), respectively;

***) A sum of both isomeric and ground states is given as predicted.

Table 2. Measured yields and mean cross-sections*) of the radionuclides formation in proton irradiation of the Ta targets of 33.3 g/cm^2 thickness at 200 and 100 MeV. The absolute yields (in atoms per proton) are given in comparison with theory.

Nuclide	200 MeV			100 MeV		
	σ, mbarn	$Y_{exp.}$	$Y_{theor.}$	σ, mbarn	$Y_{exp.}$	$Y_{theor.}$
^{182}Ta	-	$4.7\cdot10^{-4}$	-	-	$2.7\cdot10^{-4}$	-
^{179m2}Hf	0.37	$4.1\cdot10^{-5}$	$0.9\cdot10^{-3}$ **)	0.29	$1.2\cdot10^{-5}$	$1.8\cdot10^{-4}$ **)
^{178}W	32	$3.5\cdot10^{-3}$	$3.7\cdot10^{-3}$	150	$7.1\cdot10^{-3}$	$7.2\cdot10^{-3}$
^{178m2}Hf	0.30	$3.3\cdot10^{-5}$	$1.2\cdot10^{-3}$ **)	0.22	$0.94\cdot10^{-5}$	$2.2\cdot10^{-4}$ **)
^{177m}Lu	0.12	$1.3\cdot10^{-5}$	$5.3\cdot10^{-5}$ **)	0.06	$2.5\cdot10^{-6}$	$2.4\cdot10^{-6}$ **)
^{175}Hf	140	$1.5\cdot10^{-2}$	$1.2\cdot10^{-2}$	370	$1.4\cdot10^{-2}$	$0.87\cdot10^{-2}$
^{174g}Lu	1.8	$2.0\cdot10^{-4}$	} $1.8\cdot10^{-4}$	0.70	$1.8\cdot10^{-5}$	} $0.8\cdot10^{-5}$
^{174m}Lu	2.0	$2.3\cdot10^{-4}$		0.80	$2.0\cdot10^{-5}$	
^{173}Lu	116	$1.3\cdot10^{-2}$	$1.3\cdot10^{-2}$	146	$4.8\cdot10^{-3}$	$4.0\cdot10^{-3}$
^{172}Hf	110	$1.2\cdot10^{-2}$	$1.2\cdot10^{-2}$	40	$1.0\cdot10^{-3}$	$1.2\cdot10^{-3}$
^{172}Lu	5.2	$0.6\cdot10^{-3}$	$0.41\cdot10^{-3}$	2.6	$6.6\cdot10^{-5}$	$3.4\cdot10^{-5}$
^{171}Lu	130	$1.4\cdot10^{-2}$	$1.2\cdot10^{-2}$	45	$8.3\cdot10^{-4}$	$2.4\cdot10^{-4}$
^{170}Lu	120	$1.3\cdot10^{-2}$	$0.88\cdot10^{-2}$	21	$3.7\cdot10^{-4}$	$1.6\cdot10^{-4}$
^{169}Yb	93	$1.0\cdot10^{-2}$	$6.5\cdot10^{-3}$	5.5	$1.0\cdot10^{-4}$	$0.4\cdot10^{-4}$
^{168}Tm	0.30	$3.3\cdot10^{-5}$	$0.76\cdot10^{-5}$	0.18	$1.7\cdot10^{-6}$	$2\cdot10^{-7}$
^{167}Tm	29	$3.2\cdot10^{-3}$	$3.1\cdot10^{-3}$	≤0.4	$\leq3.8\cdot10^{-6}$	$1.4\cdot10^{-6}$
^{166}Dy	1.3	$1.4\cdot10^{-4}$	-	≤0.6	$\leq5.8\cdot10^{-6}$	-
^{166}Yb	11	$1.2\cdot10^{-3}$	$2.4\cdot10^{-3}$	0.5	$0.9\cdot10^{-5}$	-
^{160}Tb	≤0.15	$\leq1.7\cdot10^{-5}$	-	-	-	-
^{155}Tb	0.7	$7.8\cdot10^{-5}$	-	-	-	-
^{106m}Ag	0.013	$1.4\cdot10^{-6}$	$4\cdot10^{-7}$ **)	-	-	-
^{105}Ag	0.2	$2.2\cdot10^{-5}$	-	0.05	$1.9\cdot10^{-6}$	-
^{103}Ru	0.046	$5.1\cdot10^{-6}$	-	0.014	$5.2\cdot10^{-7}$	-
^{100}Pd	0.018	$2\cdot10^{-6}$	-	0.004	$1.5\cdot10^{-7}$	-
^{95}Nb	0.052	$5.7\cdot10^{-6}$	$2.4\cdot10^{-6}$	0.004	$1.5\cdot10^{-7}$	-
^{95}Zr	0.054	$5.9\cdot10^{-6}$	$1.2\cdot10^{-6}$	0.01	$3.8\cdot10^{-7}$	-
^{91m}Nb	0.15	$1.7\cdot10^{-5}$	$0.8\cdot10^{-6}$ **)	0.05	$1.9\cdot10^{-6}$	-
^{88}Zr	0.11	$1.2\cdot10^{-5}$	-	0.04	$1.5\cdot10^{-6}$	-
^{88}Y	0.15	$1.6\cdot10^{-5}$	-	0.07	$2.6\cdot10^{-6}$	-
^{87}Y	0.29	$3.2\cdot10^{-5}$	-	0.13	$4.9\cdot10^{-6}$	-
^{85}Sr	0.21	$2.3\cdot10^{-5}$	$4\cdot10^{-7}$	-	-	-
^{84}Rb	0.12	$1.3\cdot10^{-5}$	$1.2\cdot10^{-6}$	0.012	$4.5\cdot10^{-7}$	-
^{83}Rb	0.08	$8.8\cdot10^{-6}$	$4\cdot10^{-7}$	0.01	$3.8\cdot10^{-7}$	-
^{74}As	0.023	$2.5\cdot10^{-6}$	$1.2\cdot10^{-6}$	0.025	$9.5\cdot10^{-7}$	-
^{72}Se	0.042	$4.5\cdot10^{-6}$	-	0.016	$6.0\cdot10^{-7}$	-
^{59}Fe	0.022	$2.4\cdot10^{-6}$	$4\cdot10^{-7}$	0.004	$1.5\cdot10^{-7}$	-
^{56}Co	0.015	$1.6\cdot10^{-6}$	$4\cdot10^{-7}$	0.006	$2.3\cdot10^{-7}$	-
^{52}Mn	0.007	$7\cdot10^{-7}$	$4\cdot10^{-7}$	0.002	$0.8\cdot10^{-7}$	-
^{48}V	0.013	$1.4\cdot10^{-6}$	-	0.0016	$6.0\cdot10^{-8}$	-

*) In recalculation from measured Y to mean σ, it is assumed that effective thickness of the target is regularly shortened with the growth of a number of emitted nucleons.

**) A sum of both isomeric and ground states is given as predicted.

Table 3. Yields of radionuclides and mean cross-sections measured after activation of the ^{nat}Re target of a 21g/cm^2 thickness by 660 MeV protons. The measurement accuracy is typically better 15% with exception for some lowest yields. The theoretically predicted yield values are given in the last column.

Nuclide	$T_{1/2}$	E_γ, keV	Type of yield	Mean σ, mbarn	Yield, atoms/proton	Predicted yield
^{185}Os	93.6 d	646.1	Indep.	4.4	$3.0\cdot10^{-4}$	$4.0\cdot10^{-4}$
^{184g}Re	38 d	903.3	Indep.	38	$2.58\cdot10^{-3}$	$\}$ $3.5\cdot10^{-3}$
^{184m}Re	165 d	920.9	Indep.	11	$7.5\cdot10^{-4}$	
^{183}Re	70 d	162.5	EC cum.	62	$4.22\cdot10^{-3}$	$3.3\cdot10^{-3}$
^{182g}Re	2.67 d	1427.3	Indep.	17	$1.16\cdot10^{-3}$	$2\cdot10^{-3}$ *)
^{178}W	21.7 d	1340.9	EC cum.	36	$2.45\cdot10^{-3}$	$3.7\cdot10^{-3}$
^{182}Ta	115 d	1231.0	Indep.	2.3	$1.57\cdot10^{-4}$	$2.3\cdot10^{-4}$
^{181}Hf	42.6 d	482.0	β^- cum.	0.14	$0.95\cdot10^{-5}$	$2.1\cdot10^{-5}$
^{179m2}Hf	25.1 d	453.7	Indep.	0.12	$0.82\cdot10^{-5}$	$4.2\cdot10^{-5}$ *)
^{178m2}Hf	31 y	574.2	Indep.	0.13	$0.9\cdot10^{-5}$	$7.3\cdot10^{-5}$ *)
^{175}Hf	70 d	343.4	EC cum.	59	$4.01\cdot10^{-3}$	$4.1\cdot10^{-3}$
^{172}Hf	1.87 y	1093.6	EC cum.	55	$3.74\cdot10^{-3}$	$3.9\cdot10^{-3}$
^{177m}Lu	160.9 d	418.5	Indep.	0.034	$2.3\cdot10^{-6}$	$8\cdot10^{-6}$ *)
^{174g}Lu	3.31 y	1241.8	Indep.	0.50	$3.4\cdot10^{-5}$	$\}$ $5.2\cdot10^{-5}$
^{174m}Lu	142 d	992.0	Indep.	0.59	$4\cdot10^{-5}$	
^{173}Lu	1.37 y	272.2	EC cum.	61	$4.15\cdot10^{-3}$	$4.15\cdot10^{-3}$
^{171}Lu	8.22 d	739.8	EC cum.	46	$3.13\cdot10^{-3}$	$4.0\cdot10^{-3}$
^{170}Lu	2 d	985.1	EC cum.	42	$2.86\cdot10^{-3}$	$3.8\cdot10^{-3}$
^{169}Yb	32 d	307.7	EC cum.	57	$3.88\cdot10^{-3}$	$3.7\cdot10^{-3}$
^{166}Yb	2.36 d	1374.1	EC cum.	39	$2.65\cdot10^{-3}$	$3.6\cdot10^{-3}$
^{168}Tm	93.1 d	720.3	Indep.	0.30	$2.0\cdot10^{-5}$	$1.5\cdot10^{-5}$
^{167}Tm	9.24 d	531.5	EC cum.	50	$3.40\cdot10^{-3}$	$3.3\cdot10^{-3}$
^{166}Dy	3.4 d	1379.6	β^- cum.	≤2	$\leq1.4\cdot10^{-4}$	-
^{160}Tb	72.3 d	1271.9	Indep.	0.17	$1.2\cdot10^{-5}$	$4.2\cdot10^{-7}$
^{156}Tb	5.35 d	534.3	Indep.	0.83	$5.6\cdot10^{-5}$	$2\cdot10^{-5}$
^{155}Tb	5.32 d	367.4	EC cum.	13.4	$0.91\cdot10^{-3}$	$1.5\cdot10^{-3}$
^{153}Gd	242 d	103.2	EC cum.	13	$8.8\cdot10^{-4}$	$1.1\cdot10^{-3}$
^{151}Gd	120 d	243.2	EC cum.	12	$8.1\cdot10^{-4}$	$8.5\cdot10^{-4}$
^{149}Gd	9.4 d	298.5	EC cum.	7.4	$5.0\cdot10^{-4}$	$5.5\cdot10^{-4}$
^{146}Gd	48.3 d	633.7	EC cum.	4.5	$3.1\cdot10^{-4}$	$4.8\cdot10^{-4}$
^{156}Eu	15.2 d	2097.7	β^- cum.	0.19	$1.3\cdot10^{-5}$	-
^{149}Eu	93 d	277.0	EC cum.	8.2	$5.6\cdot10^{-4}$	$6\cdot10^{-4}$
^{148}Eu	54.5 d	550.3	Indep.	0.26	$1.8\cdot10^{-5}$	$7\cdot10^{-5}$
^{147}Eu	24.0 d	601.4	EC cum.	4.5	$3.1\cdot10^{-4}$	$6\cdot10^{-4}$
^{145}Eu	5.94 d	893.7	EC cum.	1.9	$1.3\cdot10^{-4}$	$4\cdot10^{-4}$
^{148g}Pm	5.37 d	914.9	Indep.	0.09	$0.6\cdot10^{-5}$	$\}$ $4.2\cdot10^{-7}$
^{148m}Pm	41.3 d	286.6	Indep.	0.03	$2\cdot10^{-6}$	
^{144}Pm	363 d	476.8	Indep.	0.06	$4\cdot10^{-6}$	$2.3\cdot10^{-5}$
^{143}Pm	265 d	742.0	EC cum.	1.6	$1.1\cdot10^{-4}$	$2.8\cdot10^{-4}$
^{139}Ce	137.7 d	165.8	EC cum.	0.87	$5.9\cdot10^{-5}$	-

Nuclide	$T_{1/2}$	E_γ, keV	Type of yield	Mean σ, mbarn	Yield, atoms/proton	Predicted yield
^{140}Ba	12.8 d	1596.5	β^- cum.	0.006	$0.4 \cdot 10^{-6}$	-
^{133}Ba	10.5 y	356.0	EC cum.	0.17	$1.1 \cdot 10^{-5}$	$2.7 \cdot 10^{-5}$
^{131}Ba	11.8 d	496.3	EC cum.	0.07	$5 \cdot 10^{-6}$	$1.5 \cdot 10^{-5}$
^{121m}Te	154 d	212.3	Indep.	0.15	$1.0 \cdot 10^{-5}$	$0.8 \cdot 10^{-5}$ *)
^{113}Sn	115 d	391.7	EC cum.	0.11	$7.5 \cdot 10^{-6}$	$7 \cdot 10^{-6}$
^{110m}Ag	250 d	884.7	Indep.	0.06	$4 \cdot 10^{-6}$	$3 \cdot 10^{-6}$ *)
^{106m}Ag	8.46 d	1045.8	Indep.	0.1	$7 \cdot 10^{-6}$	$4 \cdot 10^{-6}$ *)
^{105}Ag	41.3 d	443.4	EC cum.	0.13	$9 \cdot 10^{-6}$	$6 \cdot 10^{-6}$
^{103}Ru	39.3 d	497.1	β^- cum.	0.14	$0.95 \cdot 10^{-5}$	$7 \cdot 10^{-6}$
^{102}Rh	206 d	475.1	Indep.	0.12	$0.8 \cdot 10^{-5}$	$0.8 \cdot 10^{-5}$
^{100}Pd	3.6 d	2376.1	β^+ cum.	0.01	$0.7 \cdot 10^{-6}$	$3 \cdot 10^{-6}$
^{95}Nb	35 d	765.8	Indep.	0.21	$1.4 \cdot 10^{-5}$	$1.1 \cdot 10^{-5}$
^{91m}Nb	62 d	1204.8	Indep.	0.018	$1.2 \cdot 10^{-6}$	$1.7 \cdot 10^{-5}$ *)
^{95}Zr	64 d	756.7	β^- cum.	0.10	$0.7 \cdot 10^{-5}$	$5 \cdot 10^{-6}$
^{88}Zr	83.4 d	392.9	EC cum.	0.27	$1.8 \cdot 10^{-5}$	$2 \cdot 10^{-5}$
^{88}Y	106.6 d	898.0	Indep.	0.49	$3.3 \cdot 10^{-5}$	$1.7 \cdot 10^{-5}$
^{85}Sr	64.8 d	514.0	β^+ cum.	0.87	$5.9 \cdot 10^{-5}$	$2.8 \cdot 10^{-5}$
^{84}Rb	32.9 d	881.6	Indep.	0.48	$3.3 \cdot 10^{-5}$	$1.6 \cdot 10^{-5}$
^{83}Rb	86.2 d	520.4	β^+ cum.	0.75	$5.1 \cdot 10^{-5}$	$3.2 \cdot 10^{-5}$
^{75}Se	119 d	264.6	β^+ cum.	0.55	$3.7 \cdot 10^{-5}$	$2.6 \cdot 10^{-5}$
^{72}Se	8.4 d	834.0	β^+ cum.	0.2	$1.3 \cdot 10^{-5}$	$4 \cdot 10^{-6}$
^{74}As	17.8 d	595.8	Indep.	0.55	$3.7 \cdot 10^{-5}$	$1.8 \cdot 10^{-5}$
^{65}Zn	244 d	1115.8	β^+ cum.	0.30	$2 \cdot 10^{-5}$	$1.4 \cdot 10^{-5}$
^{56}Co	78.8 d	1771.4	EC cum.	0.03	$2 \cdot 10^{-6}$	$3 \cdot 10^{-6}$
^{59}Fe	44.5 d	1099.3	β^- cum.	0.24	$1.6 \cdot 10^{-5}$	$1.2 \cdot 10^{-5}$
^{54}Mn	312 d	835.3	Indep.	0.20	$1.3 \cdot 10^{-5}$	$1.4 \cdot 10^{-5}$
^{52}Mn	5.6 d	1434.1	β^+ cum.	0.022	$1.5 \cdot 10^{-6}$	$3 \cdot 10^{-6}$
^{48}V	16 d	983.5	EC cum.	0.026	$1.8 \cdot 10^{-6}$	$5 \cdot 10^{-6}$

*) A sum of independent yields of both isomeric and ground states is given as predicted.

Table 4. Comparison of the measured and predicted values of mean cross-section (mbarn) for the radionuclides detected after activation of the ^{nat}Re target by protons with an incident energy of 450, 300 and 150 MeV. The corresponding mean energy values are found to be: 433, 280 and 116 MeV, respectively.

Nuclide	450 MeV		300 MeV		150 MeV	
	exp.	theor.	exp.	theor.	exp.	theor.
^{185}Os	5.5	9.1	9.4	15	23	25
^{184g}Re	45	} 55	49	} 62	76	} 63
^{184m}Re	13		14		24	
^{183}Re	82	61	100	81	140	104
^{178}W	55	76	82	102	136	145
^{182}Ta	2.3	2.3	1.9	1.3	1.1	0.34
^{181}Hf	0.14	0.15	0.085	0.071	0.015	0.012
$^{179m2}Hf$	0.13	0.43*)	0.08	0.14*)	0.02	0.018*)
$^{178m2}Hf$	0.1	0.63*)	0.09	0.27*)	0.03	0.035*)
^{175}Hf	93	80	96	91	58	50
^{172}Hf	64	68	63	66	12	11
^{177m}Lu	0.03	0.09*)	0.024	0.022*)	0.004	-
^{174g}Lu	0.50	} 0.48	0.31	} 0.26	0.045	} 0.035
^{174m}Lu	0.68		0.47		0.07	
^{173}Lu	89	74	91	74	18	18
^{171}Lu	81	66	78	58	5.1	5.7
^{170}Lu	68	59	53	48	-	2.6
^{169}Yb	78	54	43	39	0.66	1.14
^{166}Yb	47	45	27	23	-	0.05
^{168}Tm	0.21	0.12	0.12	0.07	-	-
^{167}Tm	56	43	26	25	-	0.14
^{156}Tb	0.24	0.09	-	0.006		
^{155}Tb	8.0	6.5	-	0.28		
^{151}Gd	1.8	2.1	-	0.03		
^{149}Gd	1.5	1.3	0.18	0.007		
^{146}Gd	0.66	0.65	0.04	0.001		
^{156}Eu	0.03	-	0.07	-		
^{149}Eu	1.64	1.5	-	0.01		
^{148}Eu	0.053	0.13	0.02	-		
^{147}Eu	0.66	0.88	-	0.0007		
^{145}Eu	0.4	0.46	-	-		
^{148g}Pm	0.016	} 0.003	-	-		
^{148m}Pm	0.008		-	-		
^{144}Pm	0.011	0.018	-	0.003		
^{143}Pm	0.26	0.17	-	0.006		
^{140}Ba	0.0024	-	-	-		
^{110m}Ag	0.077	0.021*)	0.07	0.020*)	-	0.012*)
^{106m}Ag	0.17	0.015*)	0.05	0.019*)	-	-
^{105}Ag	0.24	0.056	-	0.006	0.014	-
^{103}Ru	0.10	0.046	0.12	0.020	0.08	0.006
^{95}Nb	0.20	0.075	0.17	0.056	0.058	-
^{91m}Nb	0.29	0.093*)	0.25	0.031*)	-	0.006*)

Nuclide	450 MeV		300 MeV		150 MeV	
	exp.	theor.	exp.	theor.	exp.	theor.
^{95}Zr	0.14	0.028	0.12	0.022	0.040	-
^{88}Zr	0.40	0.106	0.37	0.025	0.012	-
^{88}Y	0.34	0.10	0.22	0.022	0.043	0.006
^{85}Sr	0.69	0.162	0.54	0.009	-	-
^{84}Rb	0.45	0.075	0.31	0.034	-	-
^{83}Rb	0.87	0.146	0.51	0.047	-	-
^{75}Se	0.58	0.081	0.38	0.012	0.06	0.012
^{72}Se	0.21	0.013	0.17	-	-	-
^{74}As	0.45	0.090	0.22	0.016	-	-
^{56}Co	0.03	0.009	0.02	0.009	0.01	-
^{59}Fe	0.18	0.072	0.2	0.021	0.03	0.006
^{52}Mn	0.016	0.019	-	0.006	-	-
^{48}V	0.013	0.016	0.012	0.006	0.005	-

*) A sum of cross-section for the isomeric and ground states is given as predicted.

Table 5. Isomeric to ground state ratios for p + ^{181}Ta reaction at 660 MeV.

Isomer	I^{π}	Type of ratio	σ_m/σ_g	-ΔA
^{179m2}Hf	$25/2^-$	exp/theor*)	$3.8 \cdot 10^{-2}$	3
^{178m2}Hf	16^+	exp/theor*)	$2.1 \cdot 10^{-2}$	4
^{177m}Lu	$23/2^-$	exp/theor*)	0.093	5
^{174m}Lu	6^-	exp/exp**)	1.2	8
^{148m}Pm	6^-	exp/exp**)	1.5	34

*) Standard deviation includes the measurement error of about ±15%, while the accuracy of theory estimation is not clearly specified;

**) Standard errors of measurements are of about ±30%.

Table 6. Comparison of different variants for ^{178m2}Hf isomer production.
Mean cross-sections for the isomer and for the ^{172}Hf impurity are given.

Reaction	E_p (MeV)	Mean cross-section (mbarn)	
		^{178m2}Hf	^{172}Hf
p + Ta	660	0.31	47
p + Ta	100	0.22	40
p + Re	660	0.13	55
p + Re	150	0.03	12

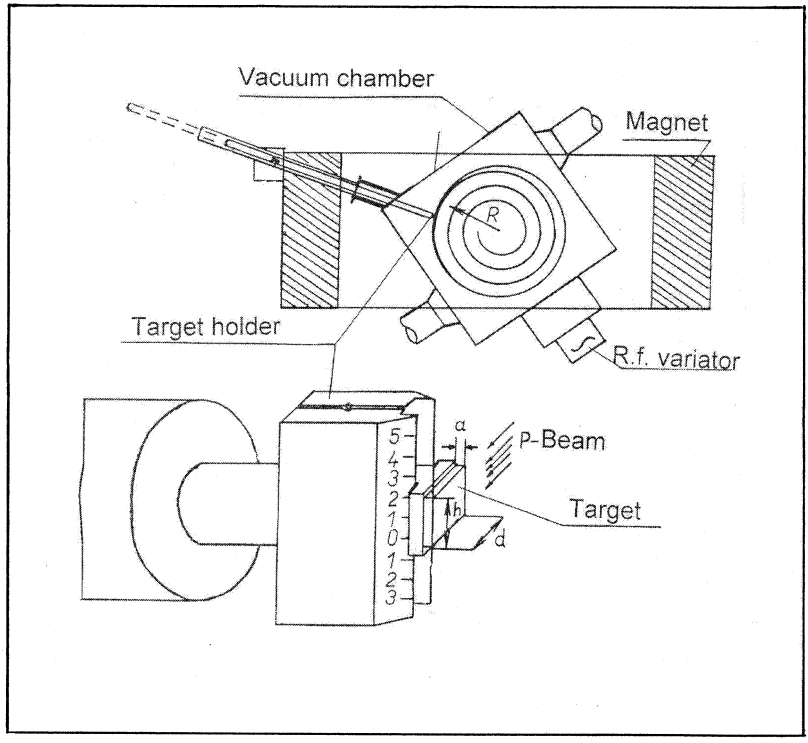

Figure 1. Synchrocyclotron LNP JINR, Dubna (Phasotron) – facility for irradiations at external and internal beams.

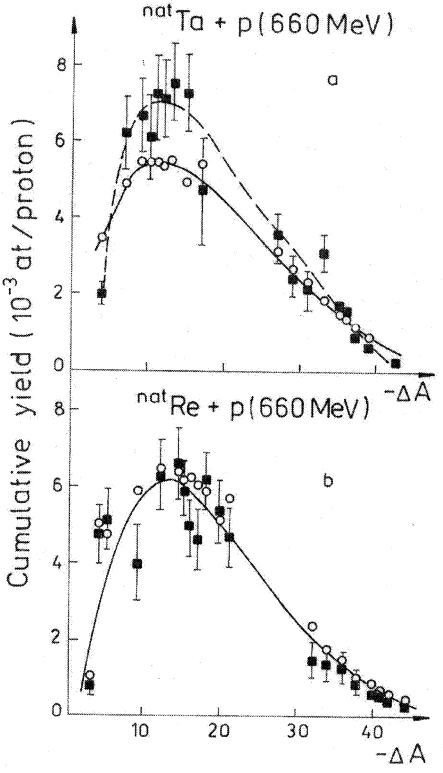

Figure 2. Mass-distributions of the cumulative yields for nuclides produced from (a) p + ^{nat}Ta and (b) p + ^{nat}Re reactions at 660 MeV. Both are reduced to the target thickness of 33.3 g/cm^2. Black squares stand for experimental results while opened circles for theory predictions. Curves are given only as guide lines.

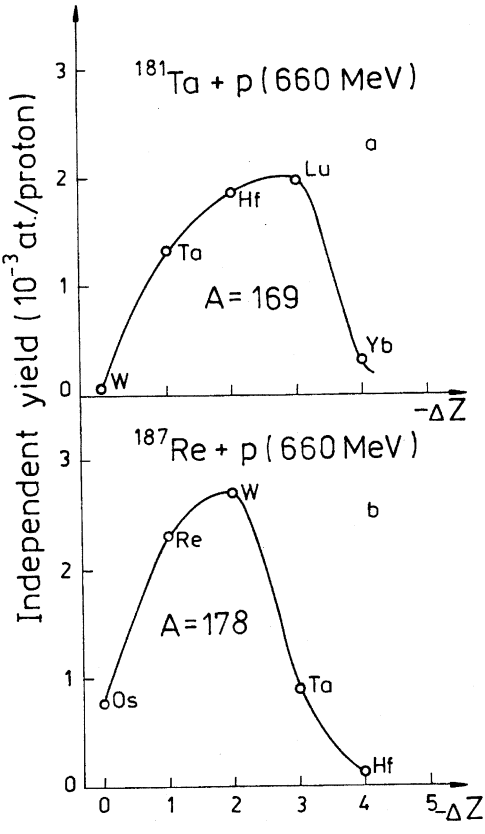

Figure 3. Isobaric charge-distributions (a) for A = 169 nuclides produced in p + ^{181}Ta reaction and (b) for A = 178 in p + ^{187}Re reaction at 660 MeV, as predicted by the numerical simulation code "LAHET".

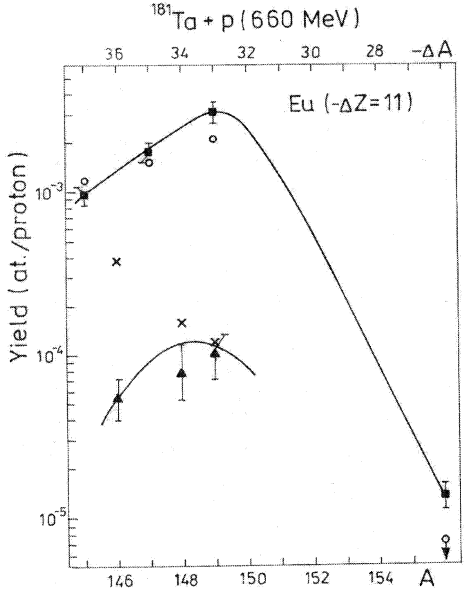

Figure 4. Isotopic distributions for Eu nuclides produced in the p + ^{181}Ta reaction at 660 MeV. Black squares and triangles correspond to the experimentally measured values for cumulative and independent yields, respectively, while opened circles and crosses correspond to the theoretically predicted ones.

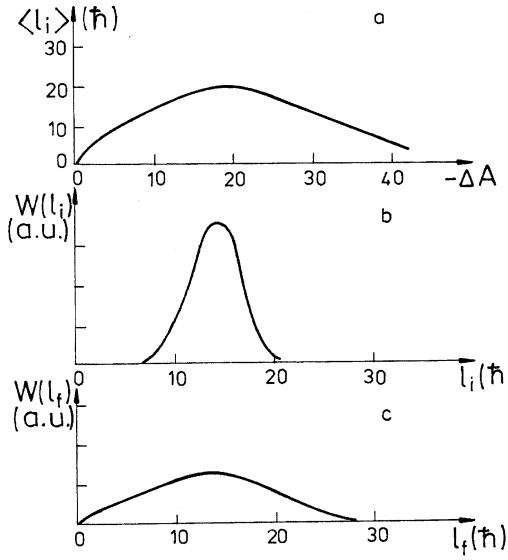

Figure 5. Results of angular momentum estimations:

a) Average angular momentum released on the first stage of the reaction as a function of (-ΔA) parameter;

b) Angular momentum distributions for (-ΔA) = 10 after the first step of the reaction;

c) The same as in b), but after the nucleon-emission stage.

References

[1] C.B.Collins, F.Davanloo, M.C.Iosif et al., Phys. Rev. Lett. 82 (1999) 695; C.B. Collins, F.Davanloo, A.C.Rusu et al., Phys. Rev. C 61 (2000) 054305.
[2] H.A.O'Brien, Nucl. Instr. and Meth. B 40/41 (1989) 1126.
[3] N.Boos, F.Le Blanc, M.Krieg et al., Phys. Rev. Lett. 72 (1994) 2689.
[4] T.Arisawa, M.Myabe, A.Sugiyama et al., Hyperfine Interactions 107 (1997) 101.
[5] J. Billowes, Nucl. Phys. A682 (2001) 206c.
[6] Yu.Ts.Oganessian, S.A.Karamian, Yu.P.Gangrski et al., Journ. of Phys., G: Nucl. and Part. Phys. 18 (1992) 393.
[7] J.B.Kim, J.Morel, M.Etcheverry et al., Journ. of Radioanalytical and Nucl. Chem. 215 (1997) 229.
[8] "Production of Radionuclides at Intermediate Energies", Subvolume C, Ed. H.Schopper, Springer-Verlag, Berlin, 1993.
[9] T.Faestermann, M.Gloris, U.Herpers et al., Annual Report of Accelerator Lab., TU Muenchen, 1998, p.45.
[10] Yu.E.Titarenko, O.V.Shvedov, M.M.Igumnov et al., Nucl. Instr. and Meth. A414 (1998) 73.
[11] N. Reus, and W. Westmeier, Atomic Data and Nuclear Tables 29 (1983) 1-192.
[12] R.B. Firestone, and V.S. Shirley, Table of Isotopes, eighth edition, J. Wiley & sons, New York 1996.
[13] C.Biratari, E.Gadioli, A.M.Grassistrini et al., Nucl. Phys. A166 (1971) 605.
[14] C.L.Rao, and L.Yaffe, Can. Journ. of Chem. 41 (1963) 2544.
[15] W.Kutschera, I.Ahmad, W.J.Childs et al., Proc. 1st Intern. Conf. on Radioactive Nucl. Beams, Berkeley, 1989, World Scientific, p.345.
[16] G.Rudstam, Z. Naturforsch, 21a (1966) 1027.
[17] P.L.Gaughey, W.Loveland, D.J.Morrisey et al., Phys. Rev. C31 (1985) 896.
[18] R.E.Prael and H.Lichtenstein, LANL Report LA-UR-89-3014 (1989).
[19] T.W.Armstrong and K.C.Chandler, Nucl. Sci. Eng. 49 (1972) 110.
[20] Y.Yariv and Z.Fraenkel, Phys. Rev. C20 (1979) 2227.
[21] K.Chen, Z.Fraenkel, G.Friedlander et al., Phys. Rev. C4 (1971) 2234.
[22] V.E.Aleksandryan, A.S.Danagulyan, L.G.Martirosyan et al., Rus. J. Nucl. Phys. 59 (1996) 592; V.E.Alexandryan, J.Adam, A.R.Balabekyan et al., Rus. J. Nucl. Phys. 63 (2000) 204.
[23] V.S.Butsev, A.S.Iljinov, and S.E.Chigrinov, Particles and Nuclei, 11 (1980) 900.
[24] V.S.Butsev, D.Chultem, and I.N.Zhivotov, Nucl. Phys. A382 (1982) 501.
[25] H.K.Vonach, R.Vandenbosch, and J.R.Huizenga, Nucl. Phys. 60 (1964) 70.
[26] S.A.Karamian, J. de Boer, Yu.Ts.Oganessian et al., Z. Phys. A356 (1996) 23.

Received by Publishing Department
on November 22, 2001.

Карамян С. А. и др.
Е6-2001-249

Получение ядер изомера ^{178m2}Hf в реакциях скалывания
при промежуточной энергии протонов на мишенях Ta и Re

Экспериментально изучена продуктивность реакций скалывания при энергиях протонов от 100 до 660 МэВ для получения радиоактивных изотопов и изомеров. С использованием методов радиохимии и гамма-спектроскопии измерены спектры мишеней Ta и Re, активированных на синхроциклотроне в Дубне. Идентифицировано большое число радиоактивных продуктов реакций скалывания и деления, их выход сравнивается с расчетом по программе LAHET. Для ядер изомеров, в частности для высокоспиновых изомеров ^{178m2}Hf, ^{179m2}Hf и ^{177m2}Lu, получены сечения σ_m и изомерные отношения σ_m / σ_g. Для понимания отношений σ_m / σ_g проведены оценки спинового распределения ядра-остатка реакции скалывания. Обсуждаются возможности оптимизации методов получения долгоживущих изомеров, поскольку это было бы необходимо для накопления таких экзотических радионуклидов в количестве миллиграммов при разумных ограничениях на стоимость и радиационную безопасность работ.

Работа выполнена в Лаборатории ядерных реакций им. Г. Н. Флерова и в Лаборатории ядерных проблем им. В. П. Джелепова ОИЯИ.

Препринт Объединенного института ядерных исследований. Дубна, 2001

Karamian S. A. et al.
E6-2001-249

Accumulation of the ^{178m2}Hf Isomeric Nuclei Through Spallation
with Intermediate-Energy Protons of Tantalum and Rhenium Targets

The productivity of the spallation reactions at proton energies of 100–660 MeV for accumulation of the radioactive isotopes and isomers has been studied experimentally. Spectra of Ta and Re targets activated at Dubna synchrocyclotron were measured using the methods of radiochemistry and gamma-spectroscopy. Many radioactive products of the spallation and fission reactions are identified, and their yields are compared with the LAHET code simulations. Cross sections, σ_m and isomer-to-ground state ratios, σ_m / σ_g are deduced for nuclear isomers, in particular, for high-spin isomers, as ^{178m2}Hf, ^{179m2}Hf and ^{177m2}Lu. Spin distributions for the spallation-residue nuclei are estimated to understand the σ_m / σ_g ratios. Possibilities to optimize the methods for the long-lived isomers production are discussed, and it would be a necessary step on the way to accumulate such exotic radionuclides in milligram amount under reasonable cost and radiation safety conditions.

The investigation has been performed at the Flerov Laboratory of Nuclear Reactions and at the Dzhelepov Laboratory of Nuclear Problems, JINR.

Preprint of the Joint Institute for Nuclear Research. Dubna, 2001

Макет Т. Е. Попеко

Подписано в печать 18.12.2001
Формат 60 × 90/16. Офсетная печать. Уч.-изд. л. 3,73
Тираж 320. Заказ 53015. Цена 4 р. 40 к.

Издательский отдел Объединенного института ядерных исследований
Дубна Московской области